Engineered symbiont biosensor maps micron-scale sugar gradients in the honeybee gut

Audam Chhun[1,*], Andrew Quinn[1], Théodora Steiner[1], Florian Zoppi[1], Thi Huong Giang Nguyen[1], Philipp Engel[1,*], Yolanda Schaerli[1,*]

[1] Department of Fundamental Microbiology, University of Lausanne, Switzerland

[*] Corresponding authors: audam.chhun@unil.ch, philipp.engel@unil.ch, yolanda.schaerli@unil.ch

Keywords: biosensor, carbohydrate, gut microbiota, *Snodgrassella alvi*, *Apis mellifera*

Abstract

The honeybee gut microbiota plays a key role in shaping host health and susceptibility to disease. Yet, the nutrient environment it experiences within the gut remains poorly characterized. In particular, little is known about the spatial distribution of nutrients across the microbial community, as resolving such fine gradients *in vivo* has been technically challenging. Here, we engineer the native honeybee symbiont *Snodgrassella alvi* as a living biosensor to quantify the bioavailability of the dietary sugar arabinose within the gut. By expanding the genetic toolkit for *S. alvi* through chromosomal integration of high-burden genes and a suite of low-strength promoters, we achieve stable multi-gene expression without compromising host colonization. The resulting biosensor generates a specific, dose-dependent fluorescent response to arabinose in the living host, enabling visualization of sugar gradients across gut-associated bacterial biofilms at micron-scale resolution. Upon co-colonization with distinct *Gilliamella* species that differ in arabinose metabolism, the biosensor reported differential *in vivo* arabinose consumption, directly validating species-specific metabolic specialization within the host. Feeding bees with pollen further uncovered pronounced radial heterogeneity in the distribution of pollen-

derived arabinose. These findings demonstrate how diet composition and microbial specialization generate fine-scale microenvironments within the gut. More broadly, this work establishes *S. alvi* as a genetically tractable platform for *in situ* biosensing, opening new avenues for dissecting metabolic interactions and nutrient distribution within living hosts.

Introduction

The honeybee serves as a tractable model to study host-microbe interactions, as their gut harbors a simple, yet specialized bacterial community[1–3]. This microbiota exerts remarkable effects on its host, influencing nutrition[4,5], pathogen resistance[6], immunity[7], detoxification[8], behavior[9,10] and cognitive development[11]. Chemical cues from both host and bacteria structure the community and govern these host-microbe and microbe-microbe interactions[12–14]. More specifically, it is the micron-scale distribution of those metabolites, rather than average levels, that dictates niche occupancy, cross-feeding and host phenotypes[15–17]. However, the gut chemical landscape remains challenging to spatially resolve *in situ*: the gastrointestinal tract is a highly dynamic, poorly accessible system with strong spatial heterogeneity.

Microsensors have profiled steep radial oxygen gradients and longitudinal pH variations at millimeter resolution in the bee gut[14]. In contrast, dietary carbohydrates, abundant from pollen and nectar, remain largely unmapped at comparable spatial scales, despite their central role in host health and disease[18,19], and in the metabolic interplay of gut symbionts[4,20]. Current insight into localized sugar bioavailability is limited to demonstrations of carbohydrate breakdown in the stomach[21], absorption in the midgut[22] and to bulk chromatography- and mass spectrometry-based measurements that average signals across gut compartments[12–14]. Such approaches lose spatial context and ignore the important micro-scale gradients that steer microbial colonization. Tools

48 capable of resolving carbohydrates *in vivo* with high spatial precision are therefore critical to
49 advance our understanding of gut microbiota function within its native context.

50 Some progress toward spatial gut chemistry has been made in mice[23] and some select
51 invertebrates[24,25] but have not been applied to insect models to the best of our knowledge. For
52 instance, spatial host-microbe sequencing and correlative mass spectrometry imaging with
53 fluorescence *in situ* hybridization have recently allowed unprecedented characterization of the
54 mouse gut microenvironments[23,26,27]. Yet, these approaches often have limited sensitivity and
55 resolution for small sugars, while requiring costly instrumentation and low throughput
56 workflows. Another strategy is to deploy engineered symbionts as live biosensors to provide fine-
57 scale, sensitive mapping of relevant metabolites directly in the gut[28,29]. In honeybees, we
58 previously engineered the core symbiont *Snodgrassella alvi* to respond to the synthetic inducer
59 IPTG, demonstrating the feasibility of cell-based sensing in this system and laying the
60 groundwork for developing biosensors for ecologically relevant carbohydrates in the bee gut
61 environment[30].

62 Previous studies identified *Gilliamella* and *Bifidobacterium* as the principal degraders of
63 complex carbohydrates in the bee gut[5]. *Gilliamella apicola* co-localizes with *S. alvi* in layered
64 biofilms, suggesting metabolic crosstalk between these species[31]. Comparative genomic and
65 metabolomic analysis indicate that they possess complementary metabolic abilities, whereby *G.*
66 *apicola* deconstructs pollen glycans and ferments released sugars to organic acids that *S. alvi*
67 consumes, in turn potentially allowing it to deplete oxygen and establish an anaerobic
68 environment for the broader community[12,13,32]. Within this carbohydrate pool, arabinose is
69 particularly interesting as high levels can be toxic to bees and only a subset of *Gilliamella* strains
70 can catabolize it[5,33]. This sugar is commonly present in the bee diet, occurring in both nectar and

71 pollen[34,35]. As such, arabinose represents a compelling target molecule for probing nutrient
72 availability and interspecies metabolic coupling.

73 Here, we expand genetic engineering capacity in *S. alvi* by introducing synthetic
74 promoters for fine control of complex circuits and a streamlined method for chromosomal
75 integration of high-burden genes, enabling *S. alvi* to function as a living biosensor for the dietary
76 sugar arabinose. The engineered strain shows a robust dose-dependent response *in vitro* and *in*
77 *vivo*, and resolves micron-scale variation in arabinose within the gut. In co-colonization with
78 *Gilliamella* strains that differ in carbohydrate metabolism, it reports arabinose consumption in a
79 controlled diet. Leveraging its sensitivity, we uncover strong radial heterogeneity in the spatial
80 distribution of arabinose derived from pollen degradation, resulting in nutrient gradients poised
81 to structure the bee gut community. Together, these results establish engineered symbionts as
82 powerful *in situ* reporters of metabolite bioavailability in the honeybee gut.

83

84 ## Results

85 **Engineering the honeybee symbiont *S. alvi* as a biosensor for arabinose**. Genetic analyses
86 previously demonstrated that *S. alvi* lacks genes for import or utilization of carbohydrates as a
87 carbon source[32]. To enable *S. alvi* to act as a biosensor for arabinose, we set out to genetically
88 reprogram it to both import and respond to this sugar *via* the expression of a fluorescent protein
89 (**Fig. 1a**).

90 To confer *S. alvi* arabinose import capability, we engineered cells to express AraE, a
91 membrane protein responsible for arabinose transport in *Escherichia coli*[36]. Membrane proteins
92 are difficult to express heterologously and prone to acquire mutations due to potential toxicity,
93 requiring tight regulation of gene expression to maintain production at low levels[37,38]. In *S. alvi*,
94 the few promoters that were available only result in high gene expression, while functional

95 plasmid replication origins replicate in medium-to-high copy number, which together often cause
96 instability in genetic circuits[30,39]. To address this limitation, we began by characterizing several
97 synthetic promoters that, although previously published[40,41], had not been evaluated in *S. alvi*. We
98 identified the CP6 promoter as promising, with respectively 70% and 50% less activity than the
99 CP25 and PA3 promoters typically used for engineering of this species[30,42] (**Supplementary Fig. 1**).
100 We then aimed to integrate the *araE* gene, driven

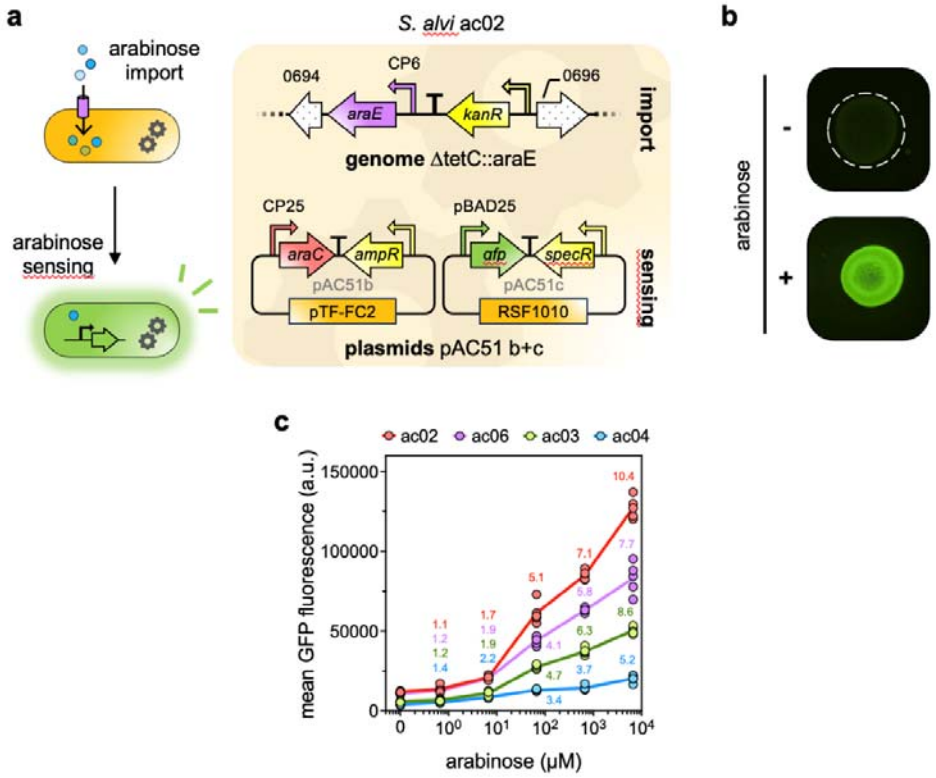

Figure 1. An engineered *S. alvi* strain detects and reports arabinose *in vitro* in a dose-dependent manner. **(a)** Overview of the genetic engineering carried out in the bee gut symbiont *S. alvi* to acquire arabinose import and sensing capabilities. The *araE* arabinose importer gene was integrated into the genome at the *tetC* locus, enabling arabinose import. Arrows filled with a dotted pattern represent neighboring genes flanking the insertion site and their gene names (SALWKB2_0694 and SALWKB2_0696) are shown above. The dual plasmid system pAC51, based on AraC-mediated regulation of the new synthetic arabinose-inducible promoter pBAD25, enabling arabinose sensing is also depicted. **(b)** Engineered *S. alvi* respond to arabinose by expressing GFP. Top-view images of bacterial lawns inoculated from 10 µl of cells (OD ~ 0.5) and grown on solid media for 3 days, with (+) or without (-) 13 mM arabinose. Dotted-

line outlines the shape of a non-fluorescent bacterial lawn. Photos were captured with a Fusion FX device (F-740 filter) using identical exposure times. (c) Variant *S. alvi* strains engineered for arabinose sensing display distinct response profiles. The graph shows mean GFP fluorescence values from 5 biological replicates. Each replicate value was obtained from the average fluorescence of at least 9,000 bacteria measured by flow cytometry. The data lines are color-coded by strain, with the corresponding strain names (ac02-ac06) shown above the plot. Mean fluorescence fold-change relative to the uninduced condition is indicated in the same color. Overview of genetic modifications for each strain can be found in Supplementary Fig. 3C.

101

102 by the CP6 promoter, into the *S. alvi* genome to minimize its copy number per cell. The
103 previously reported example of targeted genome modification in *S. alvi* used a homologous
104 recombination-based method to insert simple low-burden fluorescent reporters[43]. To achieve
105 stable genomic integration of the membrane-protein encoding *araE* gene, we built upon this
106 approach by developing a suite of standardized primers and plasmids containing different
107 antibiotic resistance cassettes, allowing straightforward and versatile gene integration in *S. alvi*
108 (**Supplementary Fig. 2a**). The constructs, referred to as suicide plasmids, are based on the
109 conditional R6K origin of replication, which functions exclusively in strains expressing the *pir*
110 gene. As a result, antibiotic-resistant *S. alvi* colonies can only arise through integration of the
111 insert fragment, rather than replication of residual plasmids originating from the initial PCR
112 reaction. We used these plasmids to pair the homology arms with an antibiotic cassette (kanR)
113 and combined them in an overlap PCR with *araE* to generate a linear fragment for the *araE*
114 knock-in. This strategy circumvented DNA replication in *E. coli*, thereby avoiding potential *araE*-
115 associated toxicity and minimizing mutation risk (see Materials and Methods and **Supplementary**
116 **Fig. 2b**). Ultimately, using this optimized genome engineering pipeline, we successfully integrated
117 a genetically stable copy of the *araE* gene into the genome of *S. alvi* (**Fig. 1a**).

118 Next, to enable *S. alvi* to detect and respond to imported arabinose, we engineered a dual
119 plasmid system in which AraC-mediated regulation drives GFP expression in response to the

120 sugar (**Fig. 1a**). In this design, *araC* and *gfp* are encoded on separate plasmids, as we previously
121 found that multi-gene constructs are genetically unstable and prone to mutations in *S. alvi*[30]. As
122 the commonly used pBAD arabinose-inducible promoter is nonfunctional in this species, we
123 designed pBAD25, a synthetic promoter variant functional in *S. alvi*, to control GFP expression
124 (**Fig. 1a**; **Supplementary Fig. 3a**). *S. alvi* was able to respond to the presence of arabinose when
125 engineered with both heterologous expression of the chromosomal *araE* gene and the synthetic
126 pBAD25 promoter (**Fig. 1b; Supplementary Fig. 3b)**. We then asked how key parameters, such as
127 AraC and AraE expression levels, as well as plasmid copy number, could modulate the cells'
128 response to arabinose. For this, we constructed four *S. alvi* strains carrying variations of our
129 genetic circuits and quantified their responses to a range of arabinose concentrations
130 (**Supplementary Fig. 3c**). Each strain displayed a distinct sugar-response profile characterized by
131 differences in dynamic range, sensitivity and basal leakiness (**Fig. 1c**). Among these, the strain *S.*
132 *alvi* ac02 exhibited the highest dynamic range and sensitivity, with fluorescence increasing up to
133 10.4-fold upon exposure to 6.7 mM arabinose relative to uninduced conditions, while maintaining
134 low levels of basal leakiness. Briefly, the strain carries a chromosomally integrated copy of the
135 *araE* importer driven by the low-strength promoter CP6, while the dual plasmid system consists
136 of a pTF-FC2-based plasmid bearing *araC* under constitutive expression from CP25 and a second
137 RSF1010-based plasmid expressing GFP under the control of the inducible promoter pBAD25
138 (**Fig. 1a**). Based on these results, we concluded that *S. alvi* ac02 was a promising candidate to sense
139 and respond in a dose-dependent manner to arabinose and pursued our work with this strain.
140

141 ***In vitro* characterization of the biosensor strain *S. alvi* ac02**. Having engineered *S. alvi* to detect
142 and respond to arabinose, we next sought to characterize *in vitro* the strain's properties relevant
143 to its function as a gut biosensor. We examined (*i*) the specificity of the response to arabinose; (*ii*)

144 the cell sensitivity to ecologically relevant sugar concentrations, and (*iii*) the stability of the
145 genetic modifications in the absence of selection pressure.

146 The engineered strain needed to distinguish arabinose from structurally related sugars.
147 The honeybee diet is indeed remarkably rich in carbohydrates, including the pentose
148 monosaccharides xylose, ribose and arabinose[33]. These sugars are stereoisomers that differ only in
149 the spatial arrangement of a hydroxyl group. To test if our biosensor responds specifically to
150 arabinose, we grew cells in media supplemented with 0.7 mM of either ribose, xylose or
151 arabinose, and measured their fluorescence levels (**Fig. 2a**). The strain responded selectively to
152 arabinose, with a 6.9-fold increase in GFP signal, while exposure to ribose or xylose resulted in
153 fluorescence levels comparable to the uninduced condition. These results indicate that the
154 engineered strain *S. alvi* ac02 provides a specific and reliable readout of arabinose in the presence
155 of structurally related carbohydrates that are found in the bee diet.

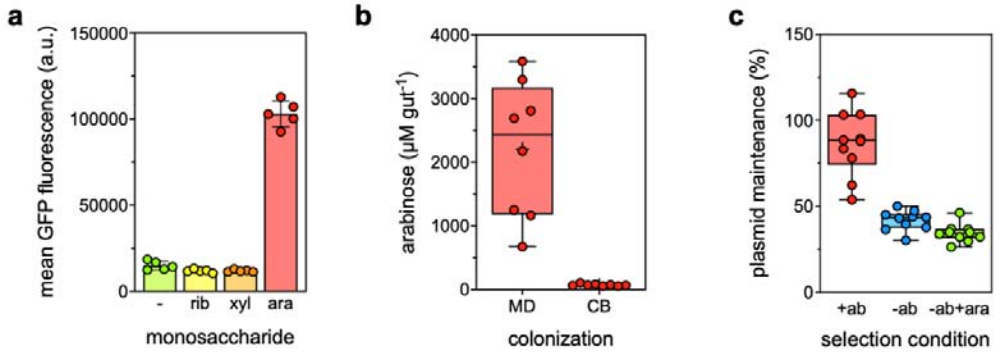

Figure 2. *In vitro* characterization of the biosensor *S. alvi* ac02 properties. (a) *S. alvi* ac02 responds specifically to arabinose. Cells were grown for 3 days in TSB alone (-) or in TSB supplemented with 0.7 mM of ribose (rib), xylose (xyl) or arabinose (ara). Bar plots show mean of GFP fluorescence ± standard deviation of 5 biological replicates. Each replicate value was obtained from the average fluorescence of at least 9,000 bacteria measured by flow cytometry. **(b)** Pollen-derived arabinose concentrations in bee guts. Bees were fed with sugar water and pollen. They were either microbiota-depleted (MD) or colonized (CB) for 7 days prior to dissection and arabinose quantification. Box plots show median arabinose concentrations measured by GC-MS and normalized with the average volume of a bee gut (n = 8). **(c)** Maintenance of arabinose-inducible plasmids pAC51b and pAC51c in *S. alvi* ac02 in the absence of

antibiotic selection. Each replicate represents a 3-day liquid culture grown in TSB with ampicillin and spectinomycin (+ab), TSB alone (-ab) or TSB with arabinose (-ab+ara). Plasmid maintenance was calculated as the fraction of CFUs growing on TSA with both antibiotics (*i.e.* cells bearing the two plasmids pAC51b and pAC51c) relative to total CFUs on non-selective TSA. Box plots show median plasmid maintenance of 10 biological replicates.

156

157 We then asked whether the biosensor could respond to sugar concentrations
158 representative of those present in the honeybee gut after pollen digestion. To determine these
159 levels, we dissected guts from pollen-fed, microbiota-deprived (MD) or colonized bees (CB),
160 homogenized them in 500 µL sterile PBS, and analyzed them by mass spectrometry
161 (**Supplementary Fig. 4a**). To convert mass spectrometry values into realistic *in vivo*
162 concentrations, we estimated the average honeybee gut volume, by measuring the mass loss of
163 water after desiccation, to be 19.1 ± 4.7 µl (see Materials and Methods and **Supplementary Fig.**
164 **4b**). Using this normalization for the gut volume, arabinose concentrations averaged 2.2 ± 1.1 mM
165 in MD bee guts, and 0.0722 ± 0.0164 mM in CB bee guts (n = 8; **Fig. 2b**). This range falls within
166 the detection window of the engineered *S. alvi* strain ac02 (**Fig. 1c**), suggesting it can report
167 variations in arabinose concentrations of both extremes: high concentrations in the absence of
168 microbial metabolism (*i.e.* MD bees) and reduced, ecologically relevant levels when the native gut
169 community consumes arabinose (*i.e.* CB bees).

170 Next, we examined the stability of the genetic circuits in the absence of antibiotics. While
171 part of the biosensor design was chromosomally integrated, we hypothesized that plasmid-borne
172 elements might be lost under non-selective conditions, as expected in the natural gut
173 environment[30]. To test this, we grew *S. alvi* ac02 in liquid tryptic soy broth (TSB) medium with
174 antibiotics (+ab), without antibiotics (-ab), or without antibiotics and arabinose supplementation
175 (-ab+ara; *i.e.* with the circuit activated) and then isolated them onto selective and non-selective
176 solid media. We quantified plasmid maintenance as the fraction of bacteria retaining both

177 plasmids (**Fig. 2c**). Under antibiotic pressure, plasmids were stably maintained whereas in its
178 absence maintenance declined to 41.7 ± 5.8 % (-ab) and 34.4 ± 5.3 % (-ab+ara). We found that loss
179 was specific to the *araC*-bearing plasmid pAC51b while the *gfp*-bearing plasmid pAC51c
180 remained stable (**Supplementary Fig. 5a**). Despite this reduction, the absolute number of plasmid-
181 bearing cells remained consequential even when they were exposed to arabinose, with an average
182 of 4.3 10^7 ± 5.3 10^6 CFU ml^{-1} (n = 10; **Supplementary Fig. 5b**), suggesting that enough bacterial
183 biosensors should remain functional in the gut environment.
184
185 **Biosensor-based mapping of arabinose distribution in the honeybee gut**. Building on the *in vitro*
186 demonstration of the biosensor's potential, we next evaluated its performance *in vivo*.
187 Specifically, we focused on whether the engineered strain could establish in the honeybee gut,
188 sense arabinose *in situ* and provide spatial information on sugar availability.
189 First, we assessed the biosensor ability to colonize the honeybee gut. For this, microbiota-
190 deprived bees were either mono-colonized with the engineered strain *S. alvi* ac02 and fed sugar
191 water with (+ab) or without antibiotics (-ab), or co-colonized with the biosensor and a native
192 undefined community derived from gut homogenate that includes wild-type *S. alvi* (-ab+gc; **Fig.**
193 **3a**). We monitored colonization dynamics by quantifying bacterial loads in fecal samples over
194 time. Results showed that even in the absence of antibiotic selection, colonization was highly
195 successful: 100% of mono-colonized bees (25 of 25 bees) and 95.6% of co-colonized bees (22 of 23
196 bees) harbored the biosensor after 7 days, with mean bacterial loads of 4.3 10^5 ± 5.7 10^5 CFU μl^{-1}
197 and 6.0 10^3 ± 9.2 10^3 CFU μl^{-1}, respectively. However, biosensor abundance declined by day 14,
198 most notably in co-colonized bees, whereas mono-colonized individuals remained colonized
199 albeit to lower bacterial loads (5.6 10^2 ± 2.3 10^3 CFU μl^{-1}, 68.2% of bee colonized).

200 Having confirmed successful colonization of the honeybee gut, we next investigated the
201 biosensor capacity to sense arabinose *in vivo*. To quantify the *in vivo* response of our biosensor,
202 we mono-colonized bees with *S. alvi* ac02 and fed them sugar water containing varying
203 concentrations of arabinose. We dissected guts and imaged them by confocal microscopy. A low
204 basal level of GFP expression in the absence of arabinose enabled straightforward identification of
205 the biosensor bacteria, even without induction. We confirmed that the engineered strain
206 successfully colonized the honeybee gut and formed biofilms that could be readily visualized (**Fig.**
207 **3b**). We then quantified fluorescence intensity with a custom FIJI pipeline that automatically
208 defined the biofilm region. The biosensor strain displayed a
209

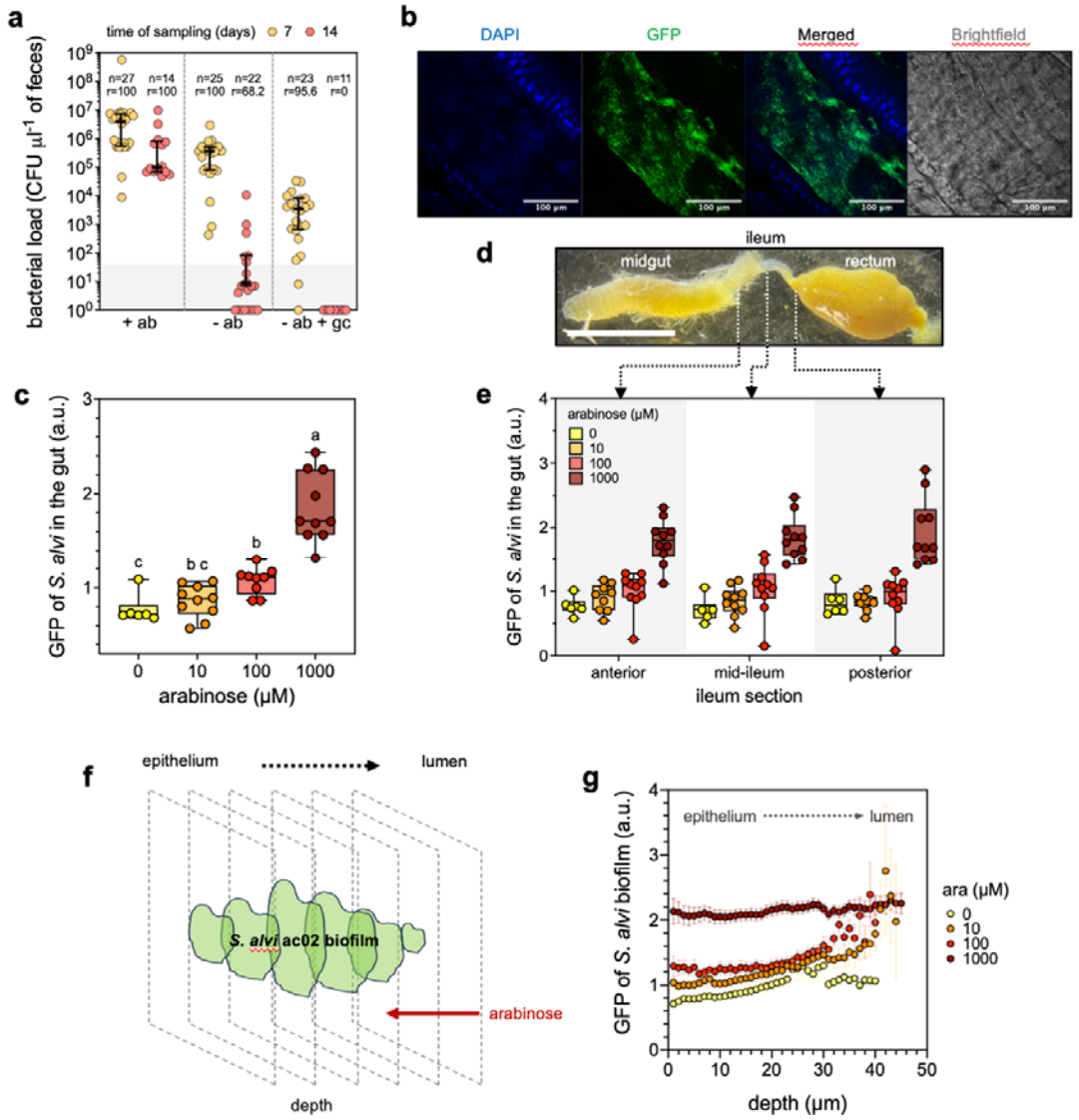

Figure 3. Engineered biosensor enables high-resolution mapping of arabinose in the honeybee gut. (a) Bacterial load of engineered *S. alvi* ac02 cells isolated from bee feces collected 7 (orange) and 14 (red) days after colonization. Bees were either mono-colonized with the biosensor strain and fed sugar water supplemented with (+ab) or without (–ab) antibiotics; or co-colonized with the biosensor strain and the native gut community (-ab+gc). Bees for which engineered bacteria were not detected in the feces were considered non-colonized. The rate of colonized bees (r) and the total number of individuals sampled (n) are indicated. For colonized bees, colored horizontal bars show median values with interquartile ranges. **(b)** A confocal microscopy image of a honeybee gut colonized by engineered *S. alvi* ac02 in the ileum region. A bacterial biofilm within a gut crypt is shown. The blue channel depicts DAPI staining of host and bacterial DNA and the green channel shows GFP fluorescence from the engineered strain. **(c)** *S. alvi* ac02 responds in a dose dependent manner to arabinose *in vivo.* Box plot shows median value of GFP fluorescence of bacterial biofilms imaged from the gut of bees fed sugar water supplemented with

indicated concentrations of arabinose (n = 10). Each fluorescence value corresponds to the average intensity measured from 3 gut sections. Different letters indicate significant differences between arabinose concentrations with adjusted *p*-value < 0.1 (Tukey HSD test) **(d)** Stereo microscopy image of a honeybee gut. The different gut regions are indicated and separated by white dotted lines. Scale bar represents 5 mm. **(e)** Sugar derived from a simple diet is homogeneously distributed along the longitudinal axis of the honeybee gut. Box plots show median value of GFP fluorescence of *S. alvi* ac02 biofilms found in different gut regions sourced from bees fed sugar water supplemented with varying concentrations of arabinose (n = 10). The regions considered were the anterior (ant) region adjoining the midgut, the mid-ileum (mid) and the posterior (post) region adjoining the rectum. **(f)** Schematic of the microscopy rationale for sugar distribution analysis across bacterial biofilm. **(g)** Sugar derived from a simple diet distributes along a gradient across the depth of *S. alvi* ac02 biofilm. Graph shows mean GFP fluorescence ± SEM of the biosensor according to the biofilm depth. For each bee (n = 10), GFP signal was first averaged over the three ileum regions. The graph displays the average of these per-bee means. Only fluorescence values for which at least two replicates could be measured for a given depth are reported.

210

211 clear dose-dependent response to arabinose, with fluorescence increasing significantly with
212 higher arabinose concentrations (**Fig. 3c**).

213 With colonization and dose-dependent sensing demonstrated, we next examined whether
214 the biosensor could resolve spatial variations in sugar availability both longitudinally (*i.e.* along
215 the length of the gut) and transversally (*i.e.* across the gut). To assess longitudinal variation,
216 fluorescence was measured in three distinct regions of the ileum: the anterior region adjoining the
217 midgut, the mid-ileum and the posterior region adjoining the rectum (**Fig. 3d**). The biosensor
218 reported fluorescence intensities consistent with the arabinose concentrations fed to the host but
219 exhibited no longitudinal variation, with similar fluorescence levels across all three regions for a
220 given sugar condition (**Fig. 3e**). These results indicate that arabinose is homogeneously distributed
221 along the ileum's length.

222 Having established longitudinal uniformity, we next asked whether arabinose availability
223 varied transversally (*i.e.* across the bacterial biofilm on the host epithelium). We hypothesized

224 that micro-scale nutrient gradients exist in these biofilms, because cells located closer to the
225 lumen typically experience higher nutrient access, while those deeper in the biofilm encounter
226 reduced concentration[44,45]. To test whether our biosensor could resolve such fine-scale gradients,
227 we performed confocal imaging with 1 μm depth increments, tracking biofilms of the engineered
228 cells from their epithelial attachment sites to the gut lumen (**Fig. 3f, Supplementary Fig. 6**). In
229 bees fed no arabinose, fluorescence remained uniform across the biofilm depth, whereas a
230 progressive increase in fluorescence toward the lumen was observed in bees fed 10 and 100 μM
231 arabinose, revealing a sugar gradient within the biofilm (**Fig. 3g**). Notably, in bees fed 1,000 μM
232 arabinose, the fluorescence signal was evenly distributed throughout the biofilm, consistent with
233 sugar saturation within the biofilm matrix. Together, these results validate the *S. alvi* biosensor as
234 a *in vivo* reporter capable of resolving transversal sugar gradients within gut biofilms, while
235 revealing longitudinal uniformity along the ileum.
236
237 ***In vivo* mapping of pollen-derived arabinose gradients in bees colonized with *Gilliamella*.** After
238 establishing that engineered *S. alvi* resolves *in vivo* arabinose gradients under a simplified diet, we
239 used it to probe the spatial distribution of pollen-derived sugar during co-colonization with
240 members of the genus *Gilliamella*.
241 Genomic analysis suggests divergent arabinose metabolism between the strains *G. apis*
242 ESL169 and *G. apicola* ESL309. The former lacks genes involved in arabinose import and
243 catabolism, whereas the latter has the gene to use this sugar as a carbon source. To visualize
244 strains *in situ*, both *Gilliamella* strains were tagged with a plasmid encoding for the fluorescent
245 reporter E2-crimson, allowing to discriminate the cells from GFP-expressing *S. alvi*. We co-
246 colonized honeybees with the *S. alvi* biosensor and either *G. apis* ESL169 or *G. apicola* ESL309
247 (**Fig. 4a**), housed the bees in cup-cages and fed them one of three diets: (*i*) simple sucrose sugar

248 water (SW), (*ii*) SW supplemented with arabinose or (*iii*) SW and pollen *ad libitum*. After 7 days,

249 we dissected the guts and imaged them by confocal microscopy. Image analysis confirmed that

250 both the *S. alvi* engineered strain and *Gilliamella* could successfully colonize the honeybee gut

251 and co-localized in the ileum as layered biofilms (**Fig. 4b**).

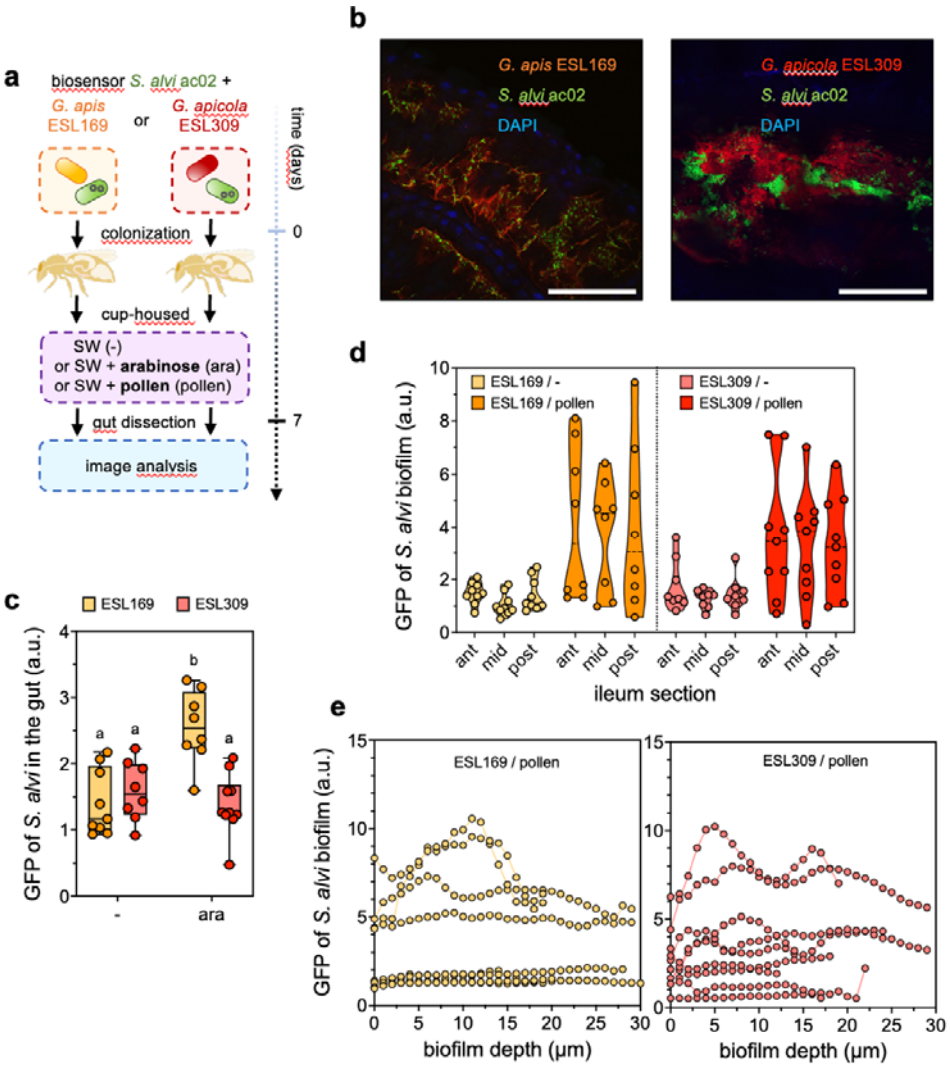

Figure 4. Biosensor mapping reveals heterogenous arabinose gradients from pollen degradation. (a) Schematic outline of the *in vivo* experiment workflow. **(b)** Confocal microscopy images of a honeybee ileum co-colonized by *S. alvi* ac02 and *G. apis* ESL169 (left) or *G. apicola* ESL309 (right). The blue channel depicts DAPI staining of host and bacterial DNA. The green channel shows GFP fluorescence from the engineered *S. alvi* strain. Red channel shows E2-crimson fluorescence from the *Gilliamella* strains transformed with the pAC09 plasmid. Scale bar represents 100 µm. **(c)** *G. apicola* ESL309 catabolizes arabinose whereas *G. apis* ESL169 does not. Box plot shows median value of GFP fluorescence

of *S. alvi* biofilms imaged from the gut of bees fed sugar water (-) or sugar water supplemented with 210 μM arabinose (ara). Each fluorescence value corresponds to the overall mean intensity averaged from 3 sections (anterior, mid-ileum, posterior) of one gut and across the depth of the bacterial biofilm for each section. Different letters indicate significant differences in fluorescence intensities across colonization and diet conditions, with adjusted p-value < 0.05 (Tukey HSD test). **(d)** Distribution of pollen-derived arabinose is longitudinally uniform along the ileum. Truncated violin plot shows median value of GFP fluorescence quantified from *S. alvi* biofilms imaged in the gut of bees fed sugar water (-) or sugar water and pollen *ad libitum* (pollen). Each fluorescence value corresponds to the mean intensity averaged across the depth of the bacterial biofilm for each gut section. **(e)** Arabinose derived from pollen breakdown distributes with high heterogeneity along a radial gradient across the depth of *S. alvi* ac02 biofilm when co-colonized with *G. apis* ESL169 (left) or *G. apicola* ESL309 (right). Graphs show the mean GFP fluorescence of the biosensor according to the biofilm depth of individual bees. Data corresponding to the anterior ileum region are displayed only for clarity. Complete data are provided in Supplementary Fig. 8.

252

253 We next aimed to confirm the metabolic abilities of the *Gilliamella* strains with regards to
254 arabinose *in vivo*. For this, we quantified *S. alvi* fluorescence across colonization states and diets.
255 The biosensor was induced only in arabinose-fed bees co-colonized with *G. apis* ESL169 (**Fig. 4c**),
256 consistent with arabinose accumulation in the gut. In contrast, no induction was observed with *G.*
257 *apicola* ESL309, indicating depletion of arabinose by the strain. These results show that the
258 biosensor can report on *in vivo* arabinose consumption and thus validate the divergent sugar
259 metabolisms of the two *Gilliamella* strains tested. Additionally, our observations provide evidence
260 that species-level differences in *Gilliamella* can influence sugar availability in the gut. Having
261 demonstrated the efficacy of the biosensor in this regard, we then leveraged it to map locally the
262 spatial distribution of pollen-derived arabinose.

263 The pollen-based diet resulted in significant induction of the biosensor, indicating the
264 accumulation of detectable levels of arabinose in the ileum, which were notably independent of
265 the *Gilliamella* species present (**Fig. 4d**). Also, fluorescence measurements of *S. alvi* along the
266 ileum's length revealed highly heterogenous arabinose concentrations between bees, although

267 homogeneously distributed longitudinally and overall consistent within each individual (**Fig. 4d;**
268 **Supplementary Fig. 7**). By contrast, depth-resolved quantification across *S. alvi* biofilms showed
269 pronounced radial heterogeneity, with arabinose availability varying sharply over microns within
270 a same biofilm and across individuals (**Fig. 4e; Supplementary Fig. 8**). Thus, while arabinose is
271 longitudinally uniform along the ileum, pollen degradation generates patchy, micron-scale
272 nutrients niches within biofilms that differ between bees. These results establish engineered
273 symbionts as sensitive, spatially precise reporters of sugar bioavailability *in vivo*, enabling
274 mapping of complex gut chemical microenvironments.
275

276 ## Discussion

277 Here, we engineered the native honeybee gut symbiont *S. alvi* as a living biosensor that
278 reports the bioavailability of the dietary sugar arabinose within the gut. By expanding the genetic
279 toolkit for *S. alvi*, we reprogrammed the bacterium to produce a specific, dose-dependent
280 response to arabinose both *in vitro* and *in vivo*, resolving micron-scale nutrient variation across
281 the gut environment. Using this system, we reveal pronounced spatial heterogeneity in arabinose
282 distribution derived from pollen degradation, uncovering nutrient gradients that likely influence
283 the spatial organization and dynamics of the bee gut microbiota. When co-colonized with distinct
284 *Gilliamella* species, the biosensor reported species-specific arabinose depletion under defined
285 dietary conditions, exposing differences in their carbohydrate metabolism.

286 Our work confirms *S. alvi* as a genetically accessible model system for functional
287 engineering of the bee gut microbiota. Although this species has been engineered before, existing
288 genetic tools could not accommodate complex circuit designs, as only a few high-expression
289 promoters were available[39]. The limited diversity of promoters forced the use of repeated identical
290 sequences across multi-gene constructs and their strong activity imposed substantial metabolic

291 burden, both factors leading to recombinations and mutations[30]. By combining chromosomal
292 integration with a suite of low-strength promoters enabling fine control of gene expression, we
293 overcome these limitations, achieving stable and predictable multi-gene expression in *S. alvi*
294 without compromising its capacity to colonize the gut. This expanded genetic control enhances
295 the tractability of *S. alvi* and broadens its potential as a chassis for *in vivo* studies and microbiome
296 engineering. Extending beyond our previous work with synthetic inducers, it now allows the
297 implementation of more complex functionalities for nutrient biosensing within the gut
298 environment.

299 The ability of an engineered honeybee symbiont to sense and report sugar *in situ* provides
300 a compelling demonstration of how synthetic approaches can provide new insights into
301 previously inaccessible features of gut chemical landscapes. Past efforts to characterize nutrient
302 distribution in animal microbiomes have largely relied on bulk chemical measurements (*i.e.* feces
303 or homogenized gut tissues) or indirect inference using techniques like metagenomics[46] or isotope
304 tracing[47]. These methods fail to capture fine-scale spatial and temporal heterogeneity. In contrast,
305 our biosensor strain enables metabolite detection within the native gut environment, preserving
306 both host and microbial context. Recent advances in spatial metabolomics, especially mass
307 spectrometry imaging, have also begun to probe metabolite distribution *in situ*, typically
308 achieving resolutions in the 3-10 μm range with commercial setups[17,24]. Notably, we could here
309 resolve sugar variation within bacterial biofilms at the 1 μm scale. By engineering biosensing
310 capabilities into a native symbiont with this spatial precision, our approach achieves finely
311 resolved nutrient detection that remains ecologically relevant within its natural niche.

312 This resolution proved particularly powerful under a simplified diet of arabinose-
313 supplemented sugar water, where it revealed a transversal arabinose gradient across bacterial
314 biofilms, with sugar being more accessible closer to the gut lumen. It also enabled the

315 discrimination of species-specific arabinose metabolism among co-colonizing *Gilliamella* species.
316 However, these metabolic differences were no longer detectable under a more complex, pollen-
317 based diet. Instead, the biosensor exposed pronounced radial heterogeneity in arabinose
318 distribution, likely arising from the continued degradation of partially digested pollen grains that
319 can be observed embedded within bacterial biofilms. These residual pollen fragments may act as
320 localized nutrient-release sites, generating patchy, micron-scale variations in sugar availability.
321 The strong heterogeneity in pollen-derived arabinose concentrations observed between bees
322 might also reflect temporal and behavioral effects. For instance, differences in how recently
323 individual bees consumed pollen prior to gut dissection or in how strongly they favored sugar
324 water *versus* pollen feeding. Regardless of its exact origin, this heterogeneity was independent of
325 the *Gilliamella* species present. This is likely due to the high overall arabinose content of pollen,
326 where small-scale depletion by individual species was insufficient to alter the biosensor's
327 response. Alternatively, the presence of pollen-derived metabolites or the limited competition for
328 substrates inherent to this two-member co-colonization may modulate *Gilliamella* metabolism
329 towards reduced arabinose utilization. Nonetheless, these observations demonstrate how diet
330 complexity and pollen breakdown can generate heterogeneous nutrient micro niches within the
331 gut, which can shape microbial interactions at fine spatial scales.

332 Our work establishes a framework for probing the spatial distribution of nutrients in the
333 honeybee gut at an unprecedented resolution, using arabinose as a model substrate. However,
334 pollen degradation releases a much broader spectrum of molecules that includes other
335 carbohydrates, proteins, lipids, amino acids and vitamins[35]. They likely form overlapping chemical
336 gradients shaping community structures and interactions. Indeed, distinct members of the
337 honeybee gut microbiota occupy different metabolic and spatial niches. *Lactobacillus* species, for
338 instance, can utilize sugar alcohols and flavonoids, whereas *Bifidobacteria* dedicate a large fraction

339 of their catabolism to the breakdown of hemicellulose and other complex polysaccharides[5,12,20].
340 Extending biosensing to these compounds, or simply to other sugars, would provide a more
341 comprehensive view of how diet composition and colonization state structures the gut's metabolic
342 environment. While arabinose has been reported to exert toxicity to honeybees at concentrations
343 more than two orders of magnitude higher than those measured in our study[48], other sugars like
344 mannose are known to adversely affect bees due to inefficient metabolism and accumulation of
345 mannose-6-phosphate[49]. Mapping the distribution and bioavailability of such sugars *in situ* could
346 therefore yield valuable insights into how specific dietary components impact gut function and
347 host physiology. In addition, the sugar composition of bee pollen varies greatly depending on
348 plant origin[50], suggesting that the nutrient landscape experienced by bees feeding on distinct
349 wildflower mixes or single-crop diets may differ substantially. Leveraging our biosensor to
350 monitor how these dietary differences shape metabolite availability would help clarify how food
351 sources could influence the gut environment. Overall, achieving this will require further
352 expansion of the *S. alvi* genetic toolkit, with sensors responsive to a broader range of metabolites
353 and genetic modules supporting more complex circuit designs. In parallel, implementing these
354 biosensors in multi-species or fully reconstituted communities will be essential to capture the
355 metabolic interplay that occurs under natural colonization conditions. Together, these advances
356 would enable high-resolution, community-level mapping of nutrient fluxes and functional
357 specialization within the honeybee gut ecosystem.

358 Finally, our findings highlight the potential of synthetic biology to bridge microbial
359 ecology and functional genomics in natural host systems. By combining genetic engineering with
360 *in situ* readouts, this work demonstrates how non-model symbionts can be transformed into
361 quantitative tools to study metabolism for microbiome research. Expanding such approaches

362 across hosts and microbial taxa will open new avenues to uncover the complex chemical dialogues
363 that underpin host-microbe symbiosis.
364

365 ## Methods

366 **Bacterial strains and culture conditions.** The honeybee gut symbionts *Snodgrassella alvi* wkB2^T
367 (ATTC No. BAA-2449), the engineered biosensor strain *S. alvi* ac02, *Gilliamella apicola* ESL309
368 and *Gilliamella apis* ESL169 were routinely cultured in Tryptic Soy Broth (TSB, Bacto BD).
369 Bacteria were grown at 34 °C under microaerophilic conditions within a 5 % CO_2 incubator, with
370 orbital shaking (170 rpm) when required. *Escherichia coli* NEB 5-α (New England Biolabs) and *E.*
371 *coli* pir+ were employed for plasmid assembly and propagation. *E. coli* strains were grown
372 aerobically in Lysogeny Broth (LB) at 37 °C with orbital shaking (220 rpm). Plasmids were
373 introduced into *S. alvi* by electroporation, and into *Gilliamella* by conjugation, following
374 previously described procedures[30]. When appropriate, antibiotics were added to culture media for
375 selection and plasmid maintenance at the following concentrations: spectinomycin, 30 - 60 μg ml^{-}
376 ^{1}; ampicillin, 30 - 100 μg ml^{-1}; and kanamycin, 25 - 50 μg ml^{-1}, depending on whether the
377 construct was maintained in *S. alvi*/*Gilliamella* or *E. coli*.
378

379 **Plasmid cloning.** To expand the genetic toolbox for *S. alvi* and enable fine-tuned gene expression,
380 we constructed a panel of plasmids carrying synthetic promoters of varying strengths sourced
381 from a previously published study[40]. Promoters CP25, CP6, CP7, CP32, CP20, J23100, J23106, and
382 J23116 were cloned into the pBTK570 backbone to generate plasmids pAC95, pAC82, pAC83,
383 pAC84, pAC85, pAC86, pAC87 and pAC88, respectively. In each case, the original PA3 promoter
384 driving *E2-crimson* in pBTK570 was replaced with the corresponding promoters using 5'
385 overhangs introduced by PCR primers. The pBTK570 backbone was amplified and linearized into

386 two fragments using the primer pairs AC436/38 and AC435/39 for CP25; AC384/38 and 386/39 for
387 CP6; AC388/38 and 387/39 for CP7; AC390/38 and 389/39 for CP32; AC392/38 and 391/39 for
388 CP20; AC394/38 and 393/39 for J23100; AC396/38 and 395/39 for J23106 and AC398/38 and
389 397/39 for J23116.

390 To generate the arabinose-responsive strains, we built the plasmids pAC51b, pAC51c,
391 pAC51g, pAC51i and pAC51j. Plasmid pAC51b was constructed by amplifying the *araC* gene from
392 pBAD33 using primers AC271 and AC272, and inserting it into the pAC17v5b backbone, which
393 was linearized into two fragments by PCR with primer pairs AC273/49 and AC274/50. Plasmid
394 pAC51c was assembled by cloning a chemically synthesized pBAD25 promoter sequence,
395 amplified with primers AC275 and AC276, into the pAC17v5a backbone, also linearized into two
396 fragments using primer pairs AC019/059 and AC022/060. Plasmid pAC51g was generated by
397 amplifying *araC* from pAC51b using primers AC507 and AC09, and inserting it into the
398 intermediate plasmid pAC51e, which was linearized with primer pairs AC59/69 and AC504/60.
399 Plasmid pAC51e itself was built by cloning the *E2-crimson* gene, amplified from pBTK570 with
400 primers AC499 and AC501, into the pAC51c backbone, which was linearized with primer pairs
401 AC503/059 and AC504/060. Plasmid pAC51i was assembled by rejoining the pAC51b backbone,
402 amplified as three fragments with primer pairs AC516/010, AC18/050 and AC049/517. During
403 amplification, the promoter CP25 was replaced by CP6 using the 5' overhang of primer AC517.
404 Plasmid pAC51j was constructed by inserting the *gfp* gene, amplified from pAC51c with primers
405 AC518 and AC009, into the pAC51b backbone linearized with primer pairs AC049/069 and
406 AC274/050.

407 To generate the standardized suicide plasmids for homologous recombination in *S. alvi*,
408 we constructed plasmids pAC62, pAC98, pAC114 and pAC115. Plasmid pAC62 was built by
409 amplifying the R6K origin of replication from pKD3 using primers AC351 and AC352 and

410 inserting it into pBTK570, which was linearized with primers AC010 and AC350. Plasmid pAC98
411 was assembled by amplifying the *kanR* cassette from pBTK519 with primers AC010 and AC447
412 and cloning it into pAC62 linearized with primers AC018 and AC448. Plasmid pAC114 was
413 generated by amplifying the *ampR* cassette from pAC08 using primers AC010 and AC541 and
414 inserting it into pAC98 linearized with primers AC018 and AC540. Plasmid pAC115 was
415 constructed by cloning the *tetR* gene, amplified from the genome of *S. alvi* using primers AC531
416 and AC532, into the pAC98 backbone linearized with primers AC533 and AC534, together with a
417 short double-stranded DNA fragment formed by annealing complementary oligonucleotides
418 AC538 and AC539.

419 Fragments were assembled using the NEBuilder HiFi DNA Assembly kit according to the
420 manufacturer guidelines. Sequences of cloning primers and synthesized DNA can be found in
421 **Supplementary Table 1** and **Supplementary Table 2**, respectively. Full plasmid maps of suicide
422 backbones and arabinose constructs are depicted in **Supplementary Fig. 2a** and **Supplementary**
423 **Fig. 3c**, respectively. The pBAD33 vector was kindly provided by Prof. David Tirrell (California
424 Institute of Technology, United States)[51]. The pAC17v5a (Addgene plasmid No. 197413),
425 pAC17v5b (No. 197414) and pAC08 (No. #197402) plasmids were previously built by our group[30].
426 The pBTK570 (No. 110615) and pBTK519 (No. 110603) plasmids were a gift from Prof. Jeffrey
427 Barrick[39]. The pKD3 (No. 45604) plasmid was a gift from Barry L. Wanner[52].

428

429 **Engineering of *S. alvi* for arabinose biosensing.** To enable *S. alvi* to import arabinose, we
430 integrated the *araE* transporter into its genome *via* homologous recombination[43]. To generate the
431 *araE* insertion construct, we first retargeted the pAC98 backbone, carrying the *kanR* cassette, to
432 the *tetC* locus. Approximately 1 kb-homology arms flanking *tetC* were amplified from the
433 genome of *S. alvi* using primer pairs AC437/438 and AC439/440, and inserted into the backbone,

434 which was linearized into two fragments using the primers AC010/216 and AC408/409
435 (**Supplementary Fig. 2**). These standardized primers can be reused for retargeting any of the
436 suicide plasmids, provided that the following constant tail sequences are appended to the primers
437 used to amplify the homology arms: 5'-cacttaacggctgacatggg-3' and 5'-catgaccaaaatcccttaacgtg-3'
438 for one arm, and 5'-cggatttacaattcgtcgtgc-3' and 5'-catctgaatcatgcgcggat-3' for the other.

439 Using the *tetC*-retargeted plasmid, we generated the final *araE* insertion fragment by
440 overlap PCR. The *araE* coding sequence was amplified from the genome of *E. coli* using primers
441 AC449/450, while the homology arms and *kanR* fragments were amplified from the retargeted
442 plasmid with primer pairs AC446/477 and AC445/462. PCR products were combined at equimolar
443 ratios (0.1 pmol each) in 20 µl of MiliQ water and assembled using 25 µl of high-fidelity DNA
444 polymerase (Phanta master mix, Vazyme). The first overlap-extension stage was performed with
445 the following conditions: 5 min at 95 °C, followed by 15 cycles of 20 sec at 95 °C, 1 min at 58 °C
446 and 2.5 min at 72 °C; and a final extension for 5 min at 72 °C. The resulting assembly was resolved
447 on an agarose gel, and the band of the expected size was gel purified. A second amplification stage
448 was then performed by mixing 2 µL of the purified overlap product with 2 µl of each of the 10 µM
449 primers AC445 and AC446, 20 µl of MiliQ water and 25 µl of high-fidelity polymerase.
450 Amplification was carried out with the following conditions: 5 min at 95 °C, 30 cycles of 20 sec at
451 95 °C, 30 sec at 58 °C and 2.5 min at 72 °C; followed by a final extension for 5 min at 72 °C.

452 The final overlap product was purified and 1 µg of linear DNA was electroporated into *S.*
453 *alvi*. Successful genomic integration of the *araE* gene was confirmed by Sanger sequencing of the
454 *tetC* locus. The resulting strain was then transformed sequentially by electroporation with
455 plasmid pAC51b followed by pAC51c, yielding the biosensor strain *S. alvi* ac02.
456

457 **Flow cytometry.** Cell fluorescence was quantified using a NovoCyte flow cytometer (Agilent) and
458 the NovoExpress software (version 1.4.1). To assess arabinose response of *S. alvi* ac02 and its
459 derivative strains, as well as measuring gene expression levels of *S. alvi* carrying the synthetic
460 low-strength promoters, single colonies were streaked as bacterial lawns on TSA plates
461 supplemented with the appropriate antibiotics and incubated for 3-4 days as described above.
462 Cells from each strain were then scraped from the agar surface, resuspended in liquid TSB to an
463 optical density of 1.0 (OD_{600} = 1), and used to inoculate five biological replicates by diluting 1:300
464 in fresh TSB supplemented with varying arabinose concentrations when required. To assess the
465 specificity of the response to arabinose, TSB was supplemented with 0.7 mM of either xylose,
466 ribose, or arabinose. After 3 days of growth, cultures were diluted 1:10 in sterile PBS for flow
467 cytometry analysis.

468 Fluorescent cells were identified using a two-step gating strategy: first, bacterial cells were
469 selected on a FSC-H/SSC-H plot; single cells were then isolated on a FSC-A/FSC-H plot.
470 Fluorescence of singlets was subsequently recorded using the FITC-H channel for GFP (ex. 488
471 nm – em. 530/30 nm) and the PE-Texas Red-H channel (ex. 561 nm – em. 615/20 nm) for E2-
472 crimson. Mean fluorescence values were calculated from a minimum of 10,000 bacterial events
473 per sample. An example of the gating strategy is provided in **Supplementary Fig. 9**.

474

475 **Determination of the honeybee gut volume.** To estimate honeybee gut volume, we quantified
476 water loss following desiccation of dissected guts from 20 bees co-colonized with *S. alvi* ac02 and
477 either *G. apicola* ESL309 or *G. apis* ESL169, collected across multiple cages from the experiment
478 described below. At day 7 post-colonization, 10 bees were sampled from the treatment in which
479 bees were fed sugar water (SW) supplemented with 210 μM arabinose, and 10 additional bees

480 were sampled from the treatment in which bees were fed SW and pollen, to assess whether pollen
481 consumption influenced gut volume.

482 Each dissected gut was transferred into a pre-weighted 1.5 ml Eppendorf tubes, and tubes
483 were weighed again to determine fresh gut mass. Tubes were then left open and placed in an oven
484 at 65 °C (fan 100%). After 22h, tubes were closed, cooled at room temperature for ~30 min,
485 reopened, and weighed to obtain the dry mass. Tubes were returned to the oven for an additional
486 4 h and weighed once more to ensure that the dry mass had stabilized. Gut volume in µl was
487 estimated assuming a density of 1 mg μl^{-1} and calculated as the mass difference between fresh and
488 dry gut weigh. As no significant difference in gut volume was observed between bees fed pollen
489 and those not fed pollen, we used the overall mean volume of 19.1 µl for subsequent calculation.
490

491 **GC-MS quantification of arabinose**. Arabinose levels in the gut were compared between MD bees
492 and those colonized with a synthetic community of 25 native bee gut bacterial strains comprising
493 the *Bartonella*, *Bifidobacterium*, *Bombilactobacillus*, *Commensalibacter*, *Frischella*, *Gilliamella*,
494 *Lactobacillus* and *Snodgrassella* genera. Bees were given sugar water and sterilized pollen *ad*
495 *libitum* for ten days. The experiment was duplicated using bees from different hives with 4 bees
496 sampled per replicate per condition. Full hindguts were collected from anesthetized bees and
497 homogenized with glass beads in 500 µl of deionized water. An aliquot of 125 µl was then
498 centrifuged for 20 min at 4 °C and 20,000 g and the supernatant was stored at -80 °C.

499 Gut homogenates and calibration curves of individual sugars were prepared identically. A
500 5 µl mixture of D-norleucine and vanillic acid internal standards was spiked into 20 µl of each
501 sample immediately before extraction with 100 µl of cold acetonitrile:methanol (1:1, v/v). Samples
502 were stored at -20 °C for 2 h, then centrifuged at 18,000 g for 20 min at 4 °C. The supernatant was
503 transferred to a new plate and dried in a speed vacuum concentrator. Samples were derivatized

504 with 50 µl of 20 mg ml^{-1} methoxyamine hydrochloride in pyridine for 90 min at 34 °C, followed
505 by 50 µl of N-Methyl-N-(trimethylsilyl)trifluoroacetamide (MSTFA) for 120 min at 45 °C.
506 Samples were then randomized and 1 µl was injected *via* autosampler into an Agilent
507 8890/5977B GC-MSD with a 2:1 split ratio and inlet temperature of 280 °C. Chromatography was
508 performed using a VF-5MS column (30 m × 0.25 mm × 0.25 µm) with 1 ml min^{-1} helium flow rate.
509 The oven was held for 2 min at 125 °C, increased at 3 °C/min to 150 °C, 5 °C/min to 225 °C, 15
510 °C/min to 300 °C, 25 °C/min to 310 °C and held for 3.3 min. The mass spectrometer was run in
511 scan mode over a mass range of 50-550 Da at a scan rate of 3.2 scans/s. Sugar peak areas were
512 quantified using Agilent MassHunter Quantitative Analysis software (version 10.0). Metabolite
513 peak areas were normalized across samples using the median internal standard areas, and a linear
514 regression curve of metabolite concentration *vs* peak area was calculated for each sugar.
515
516 **Plasmids maintenance measurement.** For the assessment of pAC51b and pAC51c stability, single
517 colonies of *S. alvi* ac02 were inoculated into liquid TSB and grown under three conditions, each
518 with 10 biological replicates: (*i*) 30 µg ml^{-1} spectinomycin, 30 µg ml^{-1} ampicillin and 25 µg ml^{-1}
519 kanamycin (+ ab); (*ii*) 25 µg ml^{-1} kanamycin only (- ab); or (*iii*) 25 µg ml^{-1} kanamycin and 0.07
520 mM arabinose (- ab + ara). After 3 days of incubation, cultures were serially diluted and plated
521 onto both selective and non-selective TSA. Plasmid maintenance was quantified as the proportion
522 of colonies that grew on selective plates relative to the total number of colonies on non-selective
523 plates, corresponding to cells maintaining both plasmids.
524
525 **Honeybee rearing and gut colonization.** Microbiota-deprived (MD) *Apis mellifera carnica* bees
526 were obtained from outdoor colonies maintained at the University of Lausanne (VD,
527 Switzerland), following previously described procedures[12]. Briefly, mature pupae were sampled

528 from brood frames and transferred to sterilized plastic emergence boxes. Pupae were incubated at
529 35 °C with 75 % humidity for 3 days. Emerging adults were supplied with sterile 1:1 (w/v) sucrose
530 solution.

531 To confirm the absence of microbial contaminants, hindguts of two newly emerged bees
532 per box were dissected and homogenized in 1 ml sterile PBS. Homogenates were plated onto
533 nutrient agar (NA), columbia blood agar (CBA), brain-heart infusion agar (BHI), LB and MRSA
534 plates and incubated under aerobic (NA, LB), microaerophilic (CBA) and anaerobic (BHI, MRSA)
535 conditions. Emergence boxes were excluded if any microbial growth was detected on the
536 corresponding plates.

537 For mono-colonization, MD bees were individually fed 5 µl of *S. alvi* ac02 resuspended at
538 OD_{600} of 0.1 in 1:1 (v/v) PBS:sucrose solution. For co-colonization with the native gut community,
539 gut homogenate stocks were prepared by pooling equal volumes of homogenized hindguts from
540 five hive bees. The colonization inoculum was generated by mixing *S. alvi* ac02 at OD_{600} of 0.1
541 with a 1:10 (v/v) dilution of the gut homogenate stock in PBS:sucrose solution. For co-
542 colonization with *G. apicola* ESL309 and *G. apis* ESL169, bees were fed a mixture containing *S.*
543 *alvi* ac02 and either of the *Gilliamella* species to a final OD_{600} of 0.1 and 1, respectively, in
544 PBS:sucrose solution. *Gilliamella* strains carried the plasmid pAC09 (Addgene plasmid No.
545 197403)[30] encoding the E2-crimson fluorescent protein to enable *in vivo* visualization.

546 Following colonization, bees were maintained in sterile cup cages at 32 °C and 75 %
547 humidity. For fecal bacterial load assays, mono-colonized bees were supplied with sugar water
548 containing 85 µM arabinose, and either 30 µg ml^{-1} ampicillin plus 30 µg ml^{-1} spectinomycin ('+ ab')
549 or no antibiotic ('- ab', '- ab + gc'). To assess the *in vivo* biosensor response to arabinose, mono-
550 colonized bees received sugar water supplemented with 30 µg ml^{-1} of each ampicillin and
551 spectinomycin, together with 0, 10, 100 or 1,000 µM arabinose. Bees co-colonized with *S. alvi*

552 ac02 and *Gilliamella* were given one of three diets: (*i*) sugar water with 60 μg ml^{-1} ampicillin, (*ii*)
553 sugar water with 60 μg ml^{-1} ampicillin and 210 μM arabinose, or (*iii*) sugar water with 60 μg ml^{-1}
554 ampicillin and pollen provided *ad libitum*.

555 As pollen autofluorescence interferes with imaging, pollen was removed from cages two
556 days prior to gut dissection. All supplemented feeding solutions (*i.e.* antibiotics and arabinose)
557 were replaced with freshly prepared solutions every 3 days to maintain consistent molecule
558 concentrations.

559

560 **Bacterial load quantification *via* fecal sampling.** To quantify the fecal abundance of *S. alvi* ac02,
561 fecal material was collected from bees at 7 and 14-day post colonization with the engineered cells.
562 Bees housed in cup cages were stunned with CO_2 and subsequently placed on ice to immobilize
563 them. While anesthetized, gentle pressure was applied manually along the abdomen from the
564 anterior end toward the stinger to induce defecation directly into the cap of sterile 1.5 ml
565 Eppendorf tubes. Samples were maintained on ice throughout the collection period.

566 Fecal matter that was sufficiently liquid was immediately serially diluted 1:10 (v/v) in
567 sterile PBS. For more viscous samples, feces were first resuspended in 4 μl of sterile PBS before
568 performing the 1:10 serial dilution. Diluted samples were plated on TSA agar supplemented with
569 30 μg ml^{-1} spectinomycin, 30 μg ml^{-1} ampicillin and 25 μg ml^{-1} kanamycin to selectively recover *S.*
570 *alvi* ac02. Colony forming unit (CFUs) were counted after 3-4 days of incubation.

571

572 **Gut microscopy analysis.** To prepare samples for microscopy, honeybee hindguts were collected
573 seven days after inoculation with engineered *S. alvi* and *Gilliamella* and immediately immersed in
574 4 % paraformaldehyde in PBS. Tissues were fixed overnight at 4 °C with gentle rotation, followed
575 by three 30-min washes at room temperature in PBS. Samples were then permeabilized and

576 stained overnight at 4 °C in the dark with 5 µg ml^{-1} 4,6-diamidino-2-phenylindole (DAPI)
577 prepared in PBS containing 1% Triton X-100. After staining, excess dye was removed by washing
578 in PBS, and the ileum was dissected, mounted in PBS and overlaid with a coverslip (number #1.5).
579 Image acquisition was performed using a Nikon AX R laser scanning confocal microscope
580 (Nikon, Japan) and the software Nikon NIS-Elements C (version 5.42.06). Images were acquired
581 with a 60X oil objective at 2048x2048 pixel format size (field of view: 294.6278x294.6278 µm) and
582 an averaging of 4 images. Pinhole size was set to 0.3 airy units, yielding an optical sectioning of
583 0.32 µm. Fluorescence acquisition was performed sequentially in two passes to minimize crosstalk:
584 E2-crimson (ex. 561 nm–em. 623-750 nm) and GFP (ex. 488 nm–em. 499-551 nm), followed
585 by DAPI (ex. 405 nm–em. 420-551 nm).
586 For quantitative fluorescence analysis, all ileums were imaged using identical laser
587 intensity and detector gain settings. For each gut, three regions were imaged: anterior, mid-ileum,
588 and posterior. For each region, Z-stacks were also collected over a maximum depth of 40 µm with
589 1 µm step increment. Fluorescence quantification was automated using a custom Fiji macro
590 developed for this study (see **Supplementary Text 1**). The macro was executed in Fiji (ImageJ2,
591 version 2.16.0). Briefly, bacterial areas were segmented by applying a GFP fluorescence threshold
592 identical across images. The resulting selected areas were copied to the corresponding DAPI
593 images. For each region, mean fluorescence intensity per unit area was extracted for both GFP
594 and DAPI channels. GFP intensities were normalized to DAPI intensities from the same
595 segmented area to account for variation in cell density. When appropriate, normalized values
596 from the three ileum regions were averaged to obtain a single fluorescence measurement per bee
597 gut.
598

599 ## Acknowledgements

600 We acknowledge Lucy Genier for her support in the laboratory with molecular biology
601 work. We thank Ly Pheak Chhun and Gonçalo Matos for helpful scientific discussions
602 throughout the project. We also thank Georgia Petsiou for assistance with the bee experiments
603 and Estelle Pignon for providing the *Gilliamella* strains bearing the pAC09 plasmid. We are
604 grateful to Silvia Moriano Gutierrez for proofreading the manuscript, and to Méline Garcia for
605 identifying the *Gilliamella* species of interest.

606 This work was supported by the University of Lausanne, the NCCR Microbiomes
607 (National Centre of Competence in Research), funded by the Swiss National Science Foundation
608 (grant no. 225148) to P.E and Y.S. The funders had no role in study design, data collection and
609 analysis, decision.

610

611 ## Author contributions

612 A.C., P.E. and Y.S. conceived the study. A.C. designed the experiments and performed molecular
613 biology work, confocal microscopy, image analysis for fluorescence quantification and bee
614 experiments with support from F.Z. Suicide plasmids were designed and built by A.C. and T.S.
615 GC-MS arabinose measurements and related bee experiments were carried out by A.Q. and
616 T.H.G.N. Y.S. and P.E. supervised the project. A.C. wrote the manuscript with input from co-
617 authors.

618

619 ## Data availability

620 The plasmids developed in this study have been deposited in Addgene and are available *via* the
621 following accession numbers: pAC62 (#249659), pAC98 (#249660), pAC114 (#249661), pAC115
622 (#249662), pAC51b (#249663) and pAC51c (#249664). Confocal microscopy images have been

623 deposited in the BioImage Archive under the accession number S-BIAD2461. Source data are
624 provided with this manuscript.
625

626 Competing interests

627 The authors declare no competing interests.
628

629 References

630 1. Martinson, V. G. *et al.* A simple and distinctive microbiota associated with honey bees and
631 bumble bees. *Mol. Ecol.* **20**, 619–628 (2011).
632 2. Engel, P., Martinson, V. G. & Moran, N. A. Functional diversity within the simple gut
633 microbiota of the honey bee. *Proc. Natl. Acad. Sci.* **109**, 11002–11007 (2012).
634 3. Kwong, W. K. & Moran, N. A. Gut microbial communities of social bees. *Nat. Rev.*
635 *Microbiol.* **14**, 374–384 (2016).
636 4. Tang, J. *et al.* Synergistic pectin deconstruction is a prerequisite for mutualistic interactions
637 between honeybee gut bacteria. *Nat. Commun.* **15**, (2024).
638 5. Zheng, H. *et al.* Division of labor in honey bee gut microbiota for plant polysaccharide
639 digestion. *Proc. Natl. Acad. Sci. U. S. A.* **116**, 25909–25916 (2019).
640 6. Steele, M. I., Motta, E. V. S., Gattu, T., Martinez, D. & Moran, N. A. The Gut Microbiota
641 Protects Bees from Invasion by a Bacterial Pathogen. *Microbiol. Spectr.* **9**, (2021).
642 7. Horak, R. D., Leonard, S. P. & Moran, N. A. Symbionts shape host innate immunity in
643 honeybees: Symbionts shape honey bee immunity. *Proc. R. Soc. B Biol. Sci.* **287**, (2020).
644 8. Sato, Y. *et al.* Insecticide resistance by a host-symbiont reciprocal detoxification. *Nat.*
645 *Commun.* **12**, 1–8 (2021).
646 9. Liberti, J. *et al.* The gut microbiota affects the social network of honeybees. *Nat. Ecol. Evol.*

647 **6**, 1471–1479 (2022).

648 10. Vernier, C. L. *et al.* Gut microbiota contribute to variations in honey bee foraging
649 intensity. *ISME J.* **18**, (2024).

650 11. Cabirol, A., Schafer, J., Neuschwander, N., Kesner, L. & Liberti, J. A defined community of
651 core gut microbiota members promotes cognitive performance in honey bees. *BioRxiv*
652 https://doi.org/10.1101/2023.01.03.522593 (2023).

653 12. Kešnerová, L. *et al.* Disentangling metabolic functions of bacteria in the honey bee gut.
654 *PLOS Biol.* **15**, 1–28 (2017).

655 13. Quinn, A. *et al.* Host-derived organic acids enable gut colonization of the honey bee
656 symbiont Snodgrassella alvi. *Nat. Microbiol.* **9**, 477–489 (2024).

657 14. Callegari, M. *et al.* Compartmentalization of bacterial and fungal microbiomes in the gut of
658 adult honeybees. *npj Biofilms Microbiomes* **7**, (2021).

659 15. Richardson, M. *et al.* SAMPL-seq reveals micron-scale spatial hubs in the human gut
660 microbiome. *Nat. Microbiol.* **10**, 527–540 (2025).

661 16. Albenberg, L. *et al.* Correlation between intraluminal oxygen gradient and radial
662 partitioning of intestinal microbiota. *Gastroenterology* **147**, 1055-1063.e8 (2014).

663 17. Stüwe, M. & Liebeke, M. From microbes to molecules: unveilinghost-microbe interactions
664 withspatial metabolomics. *Mol. Syst. Biol.* **21**, 947–951 (2025).

665 18. Zhou, G. *et al.* Honeybees fed D-galactose exhibit aging signs with changes in gut
666 microbiota and metabolism. *mSystems* **10**, (2025).

667 19. Tang, M. *et al.* Honeybee-Gilliamella synergy in carbohydrate metabolism enhances host
668 thermogenesis in cold acclimation. *npj Biofilms Microbiomes* **11**, (2025).

669 20. Brochet, S. *et al.* Niche partitioning facilitates coexistence of closely related gut bacteria.
670 *Elife* **10**, 1–23 (2021).

671 21. Oertel, E., Fieger, E. A., Williams, V. R. & Andrews, E. A. Inversion of Cane Sugar in the
672 Honey Stomach of the Bee. *J. Econ. Entomol.* **44**, 487–492 (1951).
673 22. Nicolson, S. W. The importance of osmosis in nectar secretion and its consumption by
674 insects. *Am. Zool.* **38**, 418–425 (1998).
675 23. Min, X. *et al.* Spatially resolved metabolomics: From metabolite mapping to function
676 visualising. *Clin. Transl. Med.* **14**, (2024).
677 24. Geier, B. *et al.* Spatial metabolomics of in situ host–microbe interactions at the micrometre
678 scale. *Nat. Microbiol.* **5**, (2020).
679 25. Geier, B., Oetjen, J., Ruthensteiner, B., Polikarpov, M. & Gruber-vodicka, H. R.
680 Connecting structure and function from organisms to molecules in small-animal symbioses
681 through chemo-histo-tomography. *Pnas* **118**, 1–9 (2021).
682 26. Bourceau, P. *et al.* Visualization of metabolites and microbes at high spatial resolution
683 using MALDI mass spectrometry imaging and in situ fluorescence labeling. *Nat. Protoc.* **18**,
684 3050–3079 (2023).
685 27. Lötstedt, B., Stražar, M., Xavier, R., Regev, A. & Vickovic, S. Spatial host–microbiome
686 sequencing reveals niches in the mouse gut. *Nat. Biotechnol.* **42**, 1394–1403 (2024).
687 28. Carreno, D. *et al.* Imaging of live bacterial whole-cell biosensors illuminates spatial sialic
688 acid availability within the inflamed mammalian gut. 1–45 (2024).
689 29. Rutter, J. W. *et al.* Detecting changes in the Caenorhabditis elegans intestinal environment
690 using an engineered bacterial biosensor. *ACS Synth. Biol.* **8**, 2620–2628 (2019).
691 30. Chhun, A. *et al.* An engineered bacterial symbiont allows noninvasive biosensing of the
692 honey bee gut environment. *PLoS Biol.* **22**, 1–23 (2024).
693 31. Martinson, V. G., Moy, J. & Moran, N. A. Establishment of characteristic gut bacteria
694 during development of the honeybee worker. *Appl. Environ. Microbiol.* **78**, 2830–2840

695 (2012).

696 32. Kwong, W. K., Engel, P., Koch, H. & Moran, N. A. Genomics and host specialization of
697 honey bee and bumble bee gut symbionts. *Proc. Natl. Acad. Sci. U. S. A.* **111**, 11509–11514
698 (2014).

699 33. Ricigliano, V. A. *et al.* The impact of pollen consumption on honey bee (Apis mellifera)
700 digestive physiology and carbohydrate metabolism. *Arch. Insect Biochem. Physiol.* **96**, 1–
701 14 (2017).

702 34. Nicolson, S. W. & Thornburg, R. W. *Nectar chemistry*. (Springer, 2007). doi:10.1007/978-
703 1-4020-5937-7.

704 35. Campos, M. G. R. *et al.* Pollen composition and standardisation of analytical methods . *J.*
705 *Apic. Res. Bee World* **47**, 156–163 (2008).

706 36. Kolodrubetz, D. & Schleif, R. L-Arabinose transport systems in Escherichia coli K-12. *J.*
707 *Bacteriol.* **148**, 472–479 (1981).

708 37. Wagner, S. *et al.* Consequences of membrane protein overexpression in Escherichia coli.
709 *Mol. Cell. Proteomics* **6**, 1527–1550 (2007).

710 38. Zweers, J. C., Wiegert, T. & Van Dijl, J. M. Stress-responsive systems set specific limits to
711 the overproduction of membrane proteins in Bacillus subtilis. *Appl. Environ. Microbiol.*
712 **75**, 7356–7364 (2009).

713 39. Leonard, S. P. *et al.* Genetic Engineering of Bee Gut Microbiome Bacteria with a Toolkit
714 for Modular Assembly of Broad-Host-Range Plasmids. *ACS Synth. Biol.* **7**, 1279–1290
715 (2018).

716 40. Jensen, P. R. & Hammer, K. The sequence of spacers between the consensus sequences
717 modulates the strength of prokaryotic promoters. *Appl. Environ. Microbiol.* **64**, 82–87
718 (1998).

719 41. Davis, J. H., Rubin, A. J. & Sauer, R. T. Design , construction and characterization of a set
720 of insulated bacterial promoters. *Nucleic Acids Res.* **39**, 1131–1141 (2011).
721 42. Leonard, S. P. *et al.* Engineered symbionts activate honey bee immunity and limit
722 Pathogens. *Science (80-.).* **576**, 573–576 (2020).
723 43. Lariviere, P. J. *et al.* One-step genome engineering in bee gut bacterial symbionts. *MBio* **15**,
724 (2024).
725 44. Stewart, P. S. & Franklin, M. J. Physiological heterogeneity in biofilms. *Nat. Rev.*
726 *Microbiol.* **6**, 199–210 (2008).
727 45. Stewart, P. S. *et al.* Reaction-diffusion theory explains hypoxia and heterogeneous growth
728 within microbial biofilms associated with chronic infections. *npj Biofilms Microbiomes* **2**,
729 1–8 (2016).
730 46. Tropini, C., Earle, K. A., Huang, K. C. & Sonnenburg, J. L. The Gut Microbiome□:
731 Connecting Spatial Organization to Function. *Cell Host Microbe* **21**, 433–442 (2017).
732 47. Zeng, X. *et al.* Gut bacterial nutrient preferences quantified in vivo. *Cell* **185**, 3441–3456
733 (2022).
734 48. Barker, R. J. & Lehner, Y. Influence of Diet on Sugars Found by Thin-layer
735 Chromatography in Thoraces of Honey Bees, Apis mellifera L. *J. Exp. Zool.* **188**, 157–164
736 (1974).
737 49. de la Fuente, M., Peñas, P. F. & Sols, A. Mechanism of mannose toxicity. *Biochem.*
738 *Biophys. Res. Commun.* **140**, (1986).
739 50. Liolios, V., Tananaki, C. & Dimou, M. Exploring the sugar profile of unifloral bee pollen
740 using high performance liquid chromatography. **57**, 341–350 (2018).
741 51. Kozlowski, M. T., Silverman, B. R., Johnstone, C. P. & Tirrell, D. A. Genetically
742 Programmable Microbial Assembly. *ACS Synth. Biol.* **10**, 1351–1359 (2021).

743 52. Datsenko, K. A. & Wanner, B. L. One-step inactivation of chromosomal genes in
744 Escherichia coli K-12 using PCR products. *Proc. Natl. Acad. Sci. U. S. A.* **97**, 6640–6645
745 (2000).
746